Atomic-Scale Spectroscopic Imaging of the Extreme-UV Optical Response of B and N Doped Graphene

Fredrik S. Hage, Myron D. Kapetanakis,* Juan-Carlos Idrobo, Quentin M. Ramasse* and Demie Kepaptsoglou*

Dr. F.S. Hage
SuperSTEM Laboratory, SciTech Daresbury Campus, Daresbury, WA4 4AD, U.K.

Dr. M.D. Kapetanakis
Department of Physics, University of Alabama at Birmingham, Birmingham, AL35294, U.S.A.
E-mail: myronk@uab.edu

Dr. J.-C. Idrobo
Center for Nanophase Materials Sciences, Oak Ridge National Laboratory, Oak Ridge, TN37831, U.S.A.

Prof. Q.M. Ramasse
SuperSTEM Laboratory, SciTech Daresbury Campus, Daresbury, WA4 4AD, U.K.
School of Physics and School of Chemical and Process Engineering, University of Leeds, Leeds, LS2 9JT, U.K.
E-mail: qmramasse@superstem.org

Dr. D.M. Kepaptsoglou
SuperSTEM Laboratory, SciTech Daresbury Campus, Daresbury, WA4 4AD, U.K.
York JEOL Nanocentre and Department of Physics, University of York, Heslington, York, YO10 5BR, U.K.
E-mail: dmkepap@superstem.org

Substitutional doping of graphene by impurity atoms such as boron and nitrogen, followed by atom-by-atom manipulation in the scanning transmission electron microscope, could allow for accurate tailoring of its electronic structure, plasmonic response, and even the creation of single atom devices. Beyond the identification of individual dopant atoms by means of "Z contrast" imaging, spectroscopic characterization is needed to understand the modifications induced in the electronic structure and plasmonic response. Here, atomic scale spectroscopic imaging in the extreme UV-frequency band is demonstrated. Characteristic and energy-loss-dependent contrast changes centered on individual dopant atoms are highlighted. These effects are attributed to local dopant-induced modifications of the electronic structure and are shown to be in excellent agreement with calculations of the associated densities of states.

1. Introduction

Atom-by-atom manipulation in the aberration-corrected scanning transmission electron microscope (STEM) has emerged as a promising avenue for "bottom-up" fabrication of functional nanostructures at room temperature.[1–3] Due to its one-atom-thickness, combined with (among other factors) a relatively high resistance to unintended electron beam irradiation damage in typical low-voltage STEM observation conditions, graphene is well suited as a "test-bench" for advancing electron-beam-based atom-by-atom manipulation.[3] This is evident from recent reports showing how single dopant Si atoms can be re-arranged to conform to various defect geometries in graphene using a highly focused electron beam.[2–5] Initial experimental results on electron beam manipulation of single boron, nitrogen and phosphorous dopants in graphene have also been reported,[3] suggesting that such an approach could indeed mature to the point of being a means by which various functional dopant geometries could be realized.

The initial motivation for graphene nano-structuring stemmed from studies showing that individual dopants can be used to modify the graphene's electronic structure;[6] for instance,

individual boron substitutional dopants have been shown to induce a local *p*-doped character in graphene, while individual nitrogen dopants have the opposite effect, *i.e.*, they induce an *n*-doped character.[7] This difference in behavior was shown to be, in essence, due to the very different electro-negativity of B and N compared to that of the host carbon matrix.[8] It results in local modifications of the graphene's plasmonic response,[9] increased charge carrier concentration[6,10,11] and higher on/off ratios[6] (in graphene-based field-effect transistors). Furthermore, the realization of ordered dopant superlattices within graphene, akin to the creation of quantum corals,[12] could allow for an even more specific and accurate modification of graphene's electronic properties[6,10,11,13,14] and plasmonic response.[13,15,16] This is key for optimal implementation in a wide range of proposed devices.[10,13,15–18] For instance, of immediate interest from a single-atom device perspective is the controlled realization of combined B and N single dopant configurations, following on from the recent fabrication of seamless graphene *p-n* junctions using B- and N-doped graphene at the macroscopic scale.[17] With this in mind, atom-by-atom manipulation of single atom dopants in order to controllably achieve a tailored electronic structure and/or optical response is clearly an alluring proposition.[3]

For the optimal implementation of any defect geometry in devices, a comprehensive characterization of the location and bonding of individual dopant atoms and of the induced effects on electronic structure and optical response is needed. On the one hand, "Z-contrast" high-angle annular-dark-field (HAADF) imaging allows for the atomic-scale detection and direct chemical identification of graphene defects in the STEM,[7,19,20] including the unambiguous differentiation between dopants such as B and N, as used in this work. On the other hand, electron energy loss spectroscopy (EELS) uniquely allows for characterizing the local electronic structure and dielectric response of these systems, in addition to offering an alternative, chemically-sensitive element-selective atomic-resolution imaging technique.[21]

In particular, the "core loss" region of the EEL spectrum (> ~ 50 eV) is ideal for probing the bonding of individual heteroatom defects in graphene, such as B,[7,19] N,[7,19,22,23] P,[24] and Si,[25,26] as well as single graphene edge atoms.[27] Combining such results with *ab initio* modeling allows for an in-depth analysis of defect-induced modifications of the density of unoccupied states in the structure.[7,8,23,25,26]
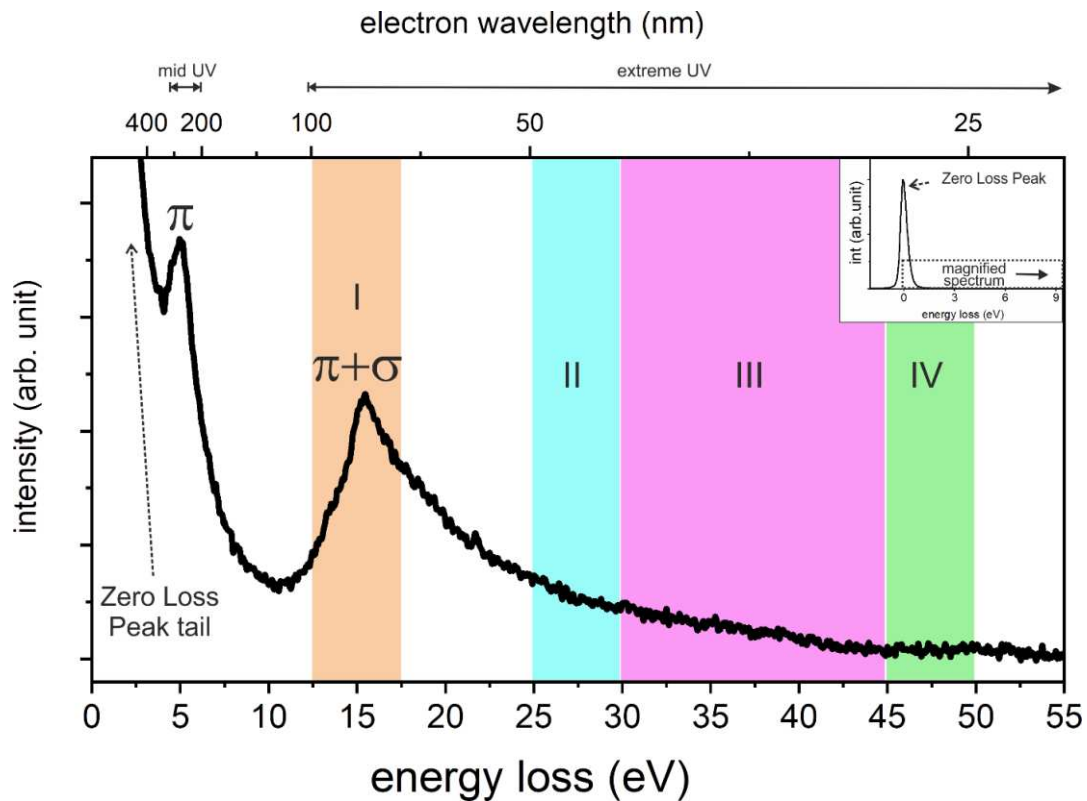
Figure 1. Experimental VEEL spectrum of (non-doped) graphene, showing the characteristic π and π+σ peaks. The colored bands (marked I-IV), drawn here as a guide to the eye, correspond to the same energy windows used for the experimental maps shown in Figure 2. Inset: zoomed out spectrum showing the Zero Loss Peak (ZLP).

Complementing this core electronic structure analysis, the ability to detect in a highly localized fashion alterations of the valence and plasmonic response of graphene at UV frequencies, which is illustrated in **Figure 1**, has been demonstrated using valence EELS (VEELS) around single Si[28,29] and, B and N dopant atoms.[9]

It was shown in particular that by integrating the spectrum intensity in the $> \sim 20$ eV loss region (extreme-UV range, Figure 1), where the relative contribution of single-electron interband transitions to the loss spectrum is significant, it is possible to create atomically-resolved energy loss lattice maps or "images" of non-doped graphene[30] and of graphene incorporating isolated substitutional Si[29] defects. The resulting atomic-resolution lattice contrast originates from the localized nature of the states involved in the interband transitions being probed by the electron beam.[30] Substitutional defects induce localized bound states as well as resonances and anti-resonances (*i.e.*, local enhancements and depletions of the density of states),[31] which also can be mapped at the atomic scale.[29] Although localized valence EELS image contrast changes centered on individual B and N dopants in graphene have also been reported, focusing in particular on mid-UV (~5eV) energies,[9] the higher frequency range is so far largely unexplored for the B- and N-doped systems.

In this report we combine experiment and theory to show that using STEM-VEELS allows for imaging the energy (loss) dependent electron structure modification induced by single substitutional B and N dopants in graphene for a range of extreme-UV frequencies with atomic resolution. Combining such measurements with a characterization of the associated plasmonic response[9,28] demonstrates how STEM-VEELS offers information of high potential value in the development of functional graphene defect geometries for potential implementation in various devices.[17,18,32–34]

5
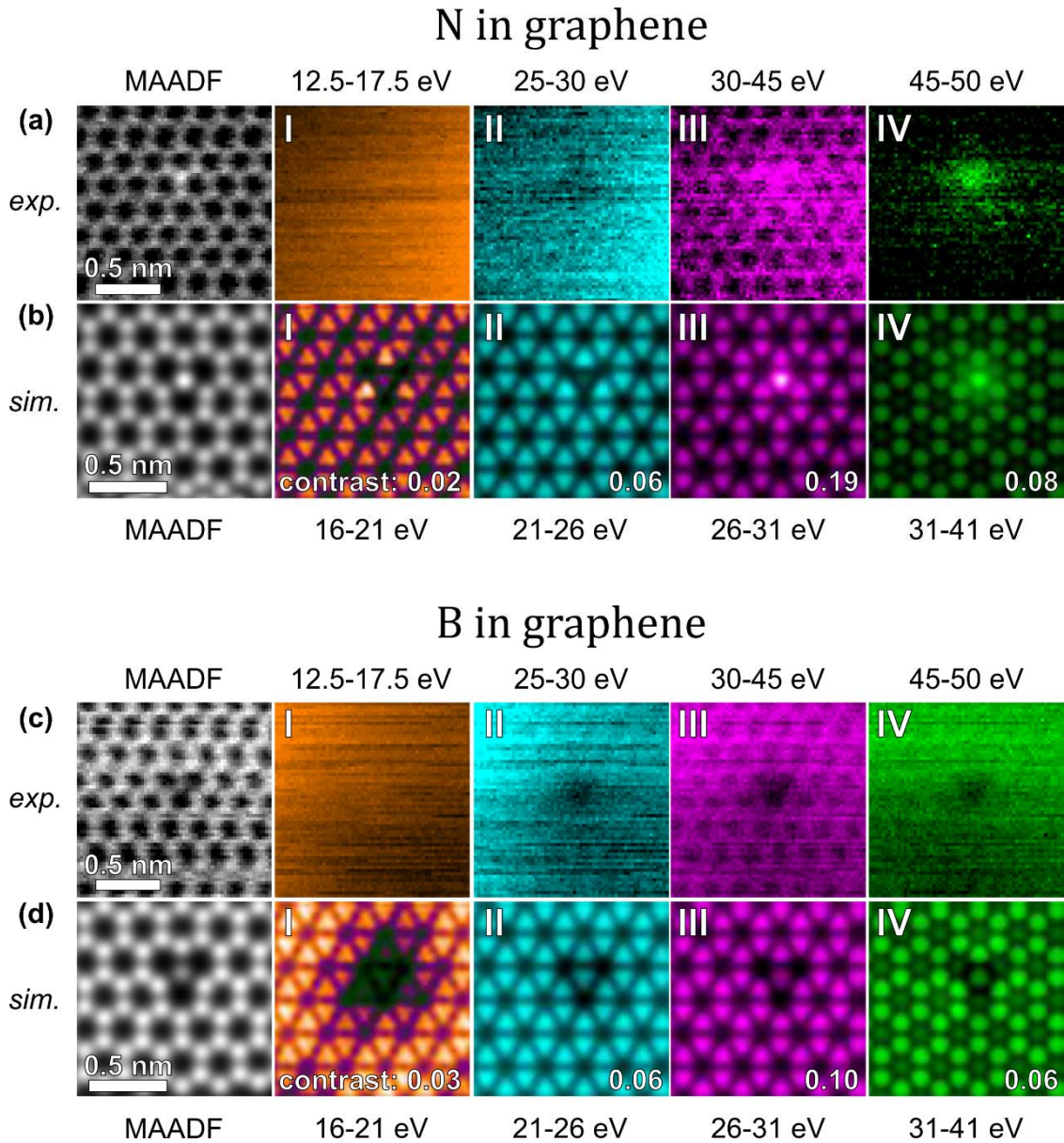
Figure 2. Experimental STEM-VEELS maps and MAADF images, encompassing either a single (a) nitrogen or (c) boron substitutional atom dopant. Corresponding simulated VEELS maps and MAADF images are shown in (b) and (d) for N- and B-doped graphene, respectively. Energy loss integration windows are indicated. The contrast values provided for each simulated VEELS map are given by $(I_{max} - I_{min}) / (I_{max} + I_{min})$ where I_{max} and I_{min} are the maximum and minimum intensity values.

2. Results and Discussion

Figure 2 shows STEM medium-angle annular-dark-field (MAADF) images and STEM-VEELS maps spanning energy losses of 12.5 – 50 eV of patches of suspended single layer graphene which contain a single substitutional N (Figure 2a) or B (Figure 2c) dopant. A comparison of these images to corresponding simulated MAADF images in Figure 2b (N) and Figure 2d (B) demonstrates the well-known ability of ADF STEM for atom-by-atom chemical identification in 2-dimensional materials: the higher (lower) contrast of the N (B) dopant clearly differs from that of the surrounding C atoms.[7,19] The corresponding simulated VEELS maps are shown in Figure 2b (N) and Figure 2d (B). The mapped energy loss regions comprise the "π+σ" peak and its extended tail (the extent of these integration windows is depicted on Figure 1 and **Figures S2** in the Supporting information provided). In STEM-VEELS experiments the nature of the π+σ peak of doped single-layer graphene is complex, but in broad terms it can be described as a superposition of two σ interband plasmons on a background of interband transitions[35-38]. The degree of collective (plasmonic) character of the peak does depend, however, on the magnitude of momentum transfer allowed to contribute to the spectrum[37], which can be controlled, e.g., by the STEM beam convergence and EELS collection angles. In the experimental conditions used here (see Experimental Section for details), the π+σ peak is expected to retain some plasmonic character but with a strong interband contribution to the overall spectrum (for further discussion of the features found in a valence electron energy loss spectrum of graphene, see References[9,35–38]).

Overall, the qualitative agreement between theory and experiment is excellent (Figure S1 in the Supporting information provided also shows a comparison of the calculated and experimental spectra). Note that uncertainties in exchange-correlation functionals red-shifts conduction band states in the calculated *ab initio* electronic structure, resulting in a slight energy mismatch of spectral features compared to experiments. For instance, the calculated

π+σ peak appears centered on 17.5 eV rather than on the experimental value of 15 eV (see Figure S1 in the Supporting information provided for further direct comparisons between experimental and theoretical spectra). Such discrepancies could be partly alleviated by adopting hybrid functionals; however, this would not affect our conclusions and is beyond the scope of the present work. In addition, calculations predict that excitonic effects contribute to the "π+σ" peak shape and absolute peak position of experimental optical absorption spectra of non-doped graphene.[39] While this suggests that excitonic effects may also play a role for experimental VEEL spectra, the inclusion of such effects in the present simulations is computationally impractical. Due to these computational restrictions, comparing calculated and experimental VEELS maps based on absolute energy loss alone is challenging. Nevertheless, a meaningful comparison between experiment and theory can be obtained by adjusting the absolute energy loss integration window ranges slightly to ensure the same spectral features contribute to the theoretical and experimental maps, and so that each theoretical map contrast best matches that of the corresponding experimental map. The integration widows used to generate the maps in Figure 2 are illustrated for convenience in Figure S2 of the Supplementary information provided. Pairs of resulting experimental and theoretical map integration windows are referred to as regions "I" to "IV" below (see also Figure 1 and Figure S2 in the Supplementary information provided).

For region I, the integration windows are centered on the π+σ peak maximum. As reported by Hage *et al.*,[9] and contrary to the case of single substitutional Si dopants,[28,29] in this energy range there is no observed localized change in contrast centered on the B and N dopants in the experimental maps. This suggests that any localized contrast in this energy loss region is significantly less pronounced than in the case of Si dopants. Additionally, caution must be taken because the experimental VEELS map contrast in this integration window can become dominated by the contribution of disordered carbonaceous material surrounding the single

layer patch. Due to the scattering physics involved, material several nm away from the probe position will contribute to the resulting spectrum (see e.g. References [9,40]); this effectively overwhelms any contribution of the more localized contrast changes predicted by theory. An illustration of the effect of adventitious carbon located on the fringes of a clean single-layer patch of graphene is provided in **Figure S3** of the Supplementary information provided.

The relative contribution of disordered carbonaceous material is lower in region II, resulting in the appearance of a weak graphene lattice contrast accompanied by a reduction in contrast centered on both individual dopant atoms.

In region III, both experimental maps exhibit a prominent graphene lattice contrast while the intensity at the B (N) atom position is lower (higher) than that of the surrounding lattice. We note that when mapping the experimental data using narrow 5 eV wide integration windows progressively spanning region III, the map contrast remains largely unchanged for both samples compared to the wider 15 eV window. The 30-45 eV map was thus deemed representative and preferred for illustration purposes thanks to its higher signal-to-noise ratio.

Lastly, in region IV, the experimental graphene lattice contrast is significantly reduced as compared to region III, resulting in the most prominent feature being the decrease (increase) in intensity centered on the B (N) atom. This is reflected in the corresponding theoretical maps, where the contrast at the center of the hexagonal rings is comparable to that at the carbon atom positions, while showing a significant decrease (increase) in intensity centered on the B (N) atom position.
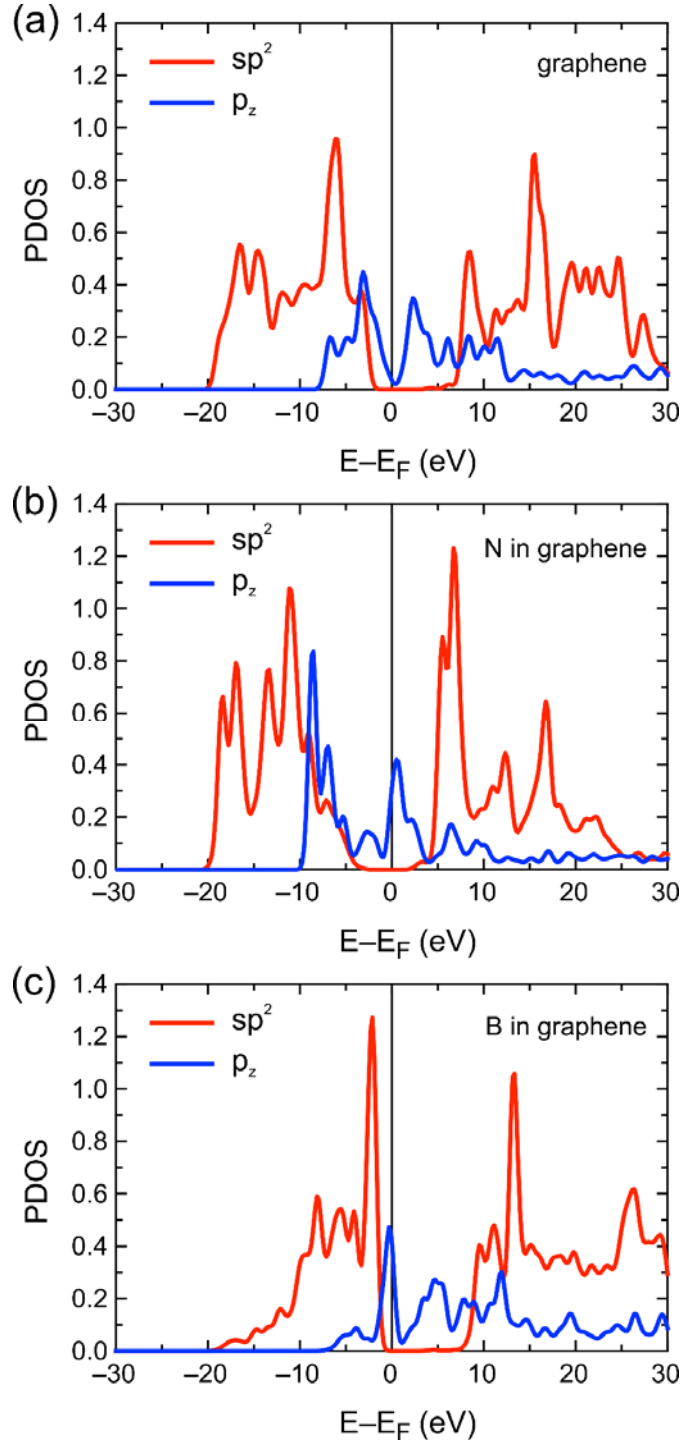
Figure 3. Calculated PDOS for (a) non-doped graphene, and graphene with a single N (b) or B (c) substitutional atom dopant. All Fermi levels are shifted to zero energy.

To understand the results in Figure 2, we need to consider the electronic states involved in the transitions contributing to the localized contrast in our maps. In **Figure 3** we show the

projected density of states (PDOS) at the dopant atom positions, plotted separately for sp^2 and p_z-like states. These compare favorably with the calculations presented in References.[7,8] We see that compared to non-doped graphene (Figure 3a), the incorporation of a single B dopant (Figure 3c) results in electronic states being pushed towards the Fermi level, while a N dopant has the opposite effect (Figure 3b). This is further visualized in the band structure calculations[7] of B- and N-doped graphene, which are presented for completeness in **Figure S4** in the Supplementary Information provided.

When calculating a VEELS map for a given energy loss, we must consider all pairs of valence and conduction states with that energy difference and take into account the width of the chosen integration window. For B-doped graphene, the observed reduction in VEELS map contrast centered on the B atom for regions II-IV can be rationalized by the predicted shift of states towards the Fermi level decreasing locally the number of conduction-valence state pairs available for interband transitions with an energy difference ≥ 25 eV. For the N-doped system, the predicted shift of states away from the Fermi level similarly explains the reduction in VEELS map contrast centered on the N atom for energy losses < 30 eV (region II) and the increase for energy losses > 30 eV (regions III and IV). Fewer (more) valence-conduction state pairs are available for interband transitions with energies of less (more) than 30 eV. For both dopant systems, the above-described effects appear to be highly localized to the dopant atom, extending at most to the closest carbon neighbors. In following with the above analysis, the reduced graphene lattice contrast in region IV maps can be attributed to the PDOS of non-doped graphene decreasing far away from the Fermi level. As discussed above, in region I, the carbonaceous material contribution to the experimental maps prevents a conclusive verification of the predicted localized reduction in contrast for both dopant systems.

Our results fit well with the prediction of localized unoccupied π* and σ* states induced by the single B and N atom dopants;[7,8] the involvement of such states in interband transitions

contributing to the VEELS signal would be expected to result, once integrated, to form maps exhibiting localized intensity changes centered on the dopant atom position akin to those we observe experimentally in Figure 2.

In a more general context, our demonstration of atomic-scale mapping of dopant-induced modifications of the electronic structure of graphene has obvious implications for the development of associated functional materials and devices. The highly focused electron beam of the STEM could be used to position single substitutional B and N atoms in such a way as to achieve very specific electronic and plasmonic properties, including the controlled opening of a (local) band gap.[14] This approach will pave the way to single-atom graphene-based field effect transistors[17,33] or solar cells.[34] Furthermore, substitutional boron and / or nitrogen doping of graphene at the macroscopic scale is also of significant interest for implementation in a wider range of graphene-based devices, not limited to nano-electronics applications. This includes for instance the elaboration of metal-free catalysts,[32] supercapacitors or Li-ion batteries.[18] It therefore falls to reason that single atom B- and N-doped graphene geometries may very well find themselves being implemented in one or more such devices in the near future. The ability to probe the electron structure down to the atomic scale, alongside complementary measurements of bonding and plasmonic response, provides analytical information that could aid the development and design of these devices, where atom-by-atom manipulation in the STEM could be used in their fabrication.

3. Conclusion

In summary, we used STEM-VEELS to image changes in electronic structure induced by single B and N dopants in graphene at the atomic scale. The incorporation of a B (N) atom pushes the density of states towards (away from) the Fermi level, resulting in energy-dependent VEELS map contrast changes in the extreme UV frequency-band. This means that

the highly focused electron beam in the STEM not only allows for atom-by-atom manipulation of defects in graphene, but also for the acquisition of detailed optical response and electronic structure data from the resulting structures, at the atomic scale. The STEM is thus truly emerging as a combined dopant manipulation and testing platform for accurate tailoring of functional single atom dopant geometries in graphene and promises to lead to the practical and controlled creation of single atom devices.

4. Experimental Section

Sample preparation: Substitutional doping was achieved by separate boron and nitrogen ion implantation of distinct graphene films supported by conventional holey carbon TEM grids, using the Göttingen mass-selected ion beam deposition system, such that two sets of (otherwise identical) samples were used for this work: one B-implanted and the other N-implanted. Further details are given in Reference[41] and references therein. The non-doped graphene reference sample is commercially available from Graphenea.[42]

STEM-EELS characterization: Experimental data was acquired using the Daresbury Nion UltraSTEM100MC dedicated scanning transmission electron microscope, equipped with a Gatan Enfinium ERS spectrometer. The operating voltage was 60 kV and the beam convergence semi-angle was 31 mrad, resulting in a 1 Å electron probe.[43] The MAADF image detector semi-angle was 59−82 mrad. The spectrometer collection semi-angle was 44 mrad. For spectra from the B and N doped samples the energy resolution (*i.e.,* the zero-loss peak – ZLP, full-width at half-maximum, FWHM) was limited by the detector point-spread function at 0.5 eV, due to the use of a spectral sampling of 0.1 eV per channel. Spectrum images of the B- and N-doped samples were acquired using Gatan's "Dual EELS" mode in order to optimize signal-to-noise in the valence loss region (see *e.g.*, Reference[9]): exposure times were 0.1 ms (for spectra including the full ZLP) and 70 ms (for spectra covering the

valence loss region only). Post-acquisition, the spectrum images of the B- and N-doped samples were de-noised using principal component analysis[44] using the 40 most significant components for reconstruction. For the spectra of the non-doped graphene reference sample in Figures 1 and S3, the energy resolution was 0.45 eV, using a spectral sampling of 0.05 eV per channel and an exposure time of 10 ms (the Dual EELS mode was not used). For the spectrum of the non-doped graphene reference sample in Figure S1, the Dual EELS mode was used: exposure times were 1 ms (for spectra including the full ZLP) and 200 ms (for spectra covering the valence loss region only). In this case, the energy resolution was 0.15 eV, using a spectral sampling of 0.05 eV per channel. No post-acquisition de-noising was used for any of the non-doped graphene spectra presented here.

Computational details: Initial and final electronic wavefunctions were calculated using Density Functional Theory (DFT) as implemented in the Vienna *ab initio* Simulations Package (VASP).[45–48] We worked within the Generalized Gradient Approximation (GGA) and took into account projector-augmented wave (PAW) corrections[45,46] (essential for proper treatment of the low momentum transfer "dipole" limit). To simulate isolated single substitutional defects, we use an expanded $5 \times 5 \times 1$ graphene supercell with 25 Å of vacuum along the z direction (to simulate the 2D nature of the system and avoid correlations between neighboring impurities due to periodicity). The Brillouin zone was sampled by using a $2 \times 2 \times 1$ k-point mesh, which was found to be sufficient for obtaining a relaxed density of states. We calculated all electronic states required in order to include all possible electronic excitations with energy-losses up to 50 eV. The energy-loss- and momentum-transfer-dependent inelastic scattering potential was calculated within the local approximation[49–51] using DFT initial and final states. Due to the absence of channeling effects for 2D systems,[29,30,51] the scattering potential is proportional to the VEELS signal. Thus, by integrating the inelastic scattering potential over particular energy loss ranges we obtain maps

that display similar spatial resolution and energy loss dependence as the experimental VEELS data. MAADF image simulations were carried out using the QSTEM[52] software package, using parameters representative of the experimental conditions.

Acknowledgements

Conflict of Interest

The authors declare no conflict of interest.

Supporting Information

Supporting Information is available from the Wiley Online Library or from the authors.

References

[1]   S. V Kalinin, S. J. Pennycook, *MRS Bull.* **2017**, *42*, 637.

[2]   O. Dyck, S. Kim, E. Jimenez-Izal, A. N. Alexandrova, S. V Kalinin, S. Jesse, *Small* **2018**, *14*, 1801771.

[3]   T. Susi, D. Kepaptsoglou, Y.-C. Y.-C. Lin, Q. M. Q. Ramasse, J. C. J. C. Meyer, K. Suenaga, J. Kotakoski, *2D Mater.* **2017**, *4*.

[4]   O. Dyck, S. Kim, S. V Kalinin, S. Jesse, *Appl. Phys. Lett.* **2017**, *111*, 113104.

[5]   M. Tripathi, A. Mittelberger, N. A. Pike, C. Mangler, J. C. Meyer, M. J. Verstraete, J. Kotakoski, T. Susi, *Nano Lett.* **2018**, *18*, 5319.

[6]   H. Terrones, R. Lv, M. Terrones, M. S. Dresselhaus, *Reports Prog. Phys.* **2012**, *75*, 62501.

[7]   D. Kepaptsoglou, T. P. Hardcastle, C. R. Seabourne, U. Bangert, R. Zan, J. A. Amani, H. Hofsäss, R. J. Nicholls, R. M. D. Brydson, A. J. Scott, Q. M. Ramasse, *ACS Nano* **2015**, *9*, 11398.

[8]   T. P. Hardcastle, C. R. Seabourne, D. M. Kepaptsoglou, T. Susi, R. J. Nicholls, R. M. D. Brydson, A. J. Scott, Q. M. Ramasse, *J. Phys. Condens. Matter* **2017**, *29*, 225303.

[9]   F. S. Hage, T. P. Hardcastle, M. N. Gjerding, D. M. Kepaptsoglou, C. R. Seabourne, K. T. Winther, R. Zan, J. A. Amani, H. C. Hofsaess, U. Bangert, K. S. Thygesen, Q. M. Ramasse, *ACS Nano* **2018**, *12*, 1837.

[10]   H. Lee, K. Paeng, I. S. Kim, A review of doping modulation in graphene. *Synth. Met.* **2018**, *244*, 36–47.

[11]   T. Wu, H. Shen, L. Sun, B. Cheng, B. Liu, J. Shen, *New J. Chem.* **2012**, *36*, 1385.

[12]   M. F. Crommie, C. P. Lutz, D. M. Eigler, *Science (80-.).* **1993**, *262*, 218.

[13]   K. S. Novoselov, V. I. Fal′ko, L. Colombo, P. R. Gellert, M. G. Schwab, K. Kim, *Nature* **2012**, *490*, 192.

[14]   S. Casolo, R. Martinazzo, G. F. Tantardini, *J. Phys. Chem. C* **2011**, *115*, 3250.

[15]   F. J. García de Abajo, *ACS Photonics* **2014**, *1*, 135.

[16]   A. N. Grigorenko, M. Polini, K. S. Novoselov, *Nat. Photon.* **2012**, *6*, 749.

[17]   G. Wang, M. Zhang, D. Chen, Q. Guo, X. Feng, T. Niu, X. Liu, A. Li, J. Lai, D. Sun, Z. Liao, Y. Wang, P. K. Chu, G. Ding, X. Xie, Z. Di, X. Wang, *Nat. Commun.* **2018**, *9*, 5168.

[18]   U. N. Maiti, W. J. Lee, J. M. Lee, Y. Oh, J. Y. Kim, J. E. Kim, J. Shim, T. H. Han, S. O. Kim, 25th anniversary article: Chemically modified/doped carbon nanotubes & graphene for optimized nanostructures & nanodevices. *Adv. Mater.* **2014**, *26*, 40–67.

[19]   U. Bangert, W. Pierce, D. M. Kepaptsoglou, Q. Ramasse, R. Zan, M. H. Gass, J. A. Van den Berg, C. B. Boothroyd, J. Amani, H. Hofsäss, *Nano Lett.* **2013**, *13*, 4902.

[20]   O. L. Krivanek, M. F. Chisholm, V. Nicolosi, T. J. Pennycook, G. J. Corbin, N. Dellby, M. F. Murfitt, C. S. Own, Z. S. Szilagyi, M. P. Oxley, S. T. Pantelides, S. J. Pennycook, *Nature* **2010**, *464*, 571.

[21]   K. Suenaga, Y. Sato, Z. Liu, H. Kataura, T. Okazaki, K. Kimoto, H. Sawada, T. Sasaki, K. Omoto, T. Tomita, T. Kaneyama, Y. Kondo, *Nat Chem* **2009**, *1*, 415.

[22]   J. H. Warner, Z. Liu, K. He, A. W. Robertson, K. Suenaga, *Nano Lett.* **2013**, *13*, 4820.

[23]   R. J. Nicholls, A. T. Murdock, J. Tsang, J. Britton, T. J. Pennycook, A. Koós, P. D. Nellist, N. Grobert, J. R. Yates, *ACS Nano* **2013**, *7*, 7145.

[24]   T. Susi, T. P. Hardcastle, H. Hofsäss, A. Mittelberger, T. J. Pennycook, C. Mangler, R. Drummond-Brydson, A. J. Scott, J. C. Meyer, J. Kotakoski, *2D Mater.* **2017**, *4*, 21013.

[25] Q. M. M. Ramasse, C. R. R. Seabourne, D.-M. Kepaptsoglou, R. Zan, U. Bangert, A. J. J. Scott, *Nano Lett.* **2013**, *13*, 4989.

[26] W. Zhou, M. D. Kapetanakis, M. P. Prange, S. T. Pantelides, S. J. Pennycook, J.-C. Idrobo, *Phys. Rev. Lett.* **2012**, *109*, 206803.

[27] K. Suenaga, M. Koshino, *Nature* **2010**, *468*, 1088.

[28] W. Zhou, J. Lee, J. Nanda, S. T. Pantelides, S. J. Pennycook, J.-C. Idrobo, *Nat. Nano.* **2012**, *7*, 161.

[29] M. D. Kapetanakis, M. P. Oxley, W. Zhou, S. J. Pennycook, J.-C. Idrobo, S. T. Pantelides, *Phys. Rev. B* **2016**, *94*, 155449.

[30] M. D. Kapetanakis, W. Zhou, M. P. Oxley, J. Lee, M. P. Prange, S. J. Pennycook, J. C. Idrobo, S. T. Pantelides, *Phys. Rev. B* **2015**, *92*, 125147.

[31] J. Bernholc, N. O. Lipari, S. T. Pantelides, *Phys. Rev. Lett.* **1978**, *41*, 895.

[32] C. Hu, L. Dai, *Adv. Mater.* **2019**, *31*, 1804672.

[33] J. Li, L. Niu, Z. Zheng, F. Yan, *Adv. Mater.* **2014**, *26*, 5239.

[34] M. Hadadian, J.-P. Correa-Baena, E. K. Goharshadi, A. Ummadisingu, J.-Y. Seo, J. Luo, S. Gholipour, S. M. Zakeeruddin, M. Saliba, A. Abate, M. Grätzel, A. Hagfeldt, *Adv. Mater.* **2016**, *28*, 8681.

[35] D. Novko, V. Despoja, M. Šunjić, *Phys. Rev. B - Condens. Matter Mater. Phys.* **2015**, *91*, 195407.

[36] V. U. Nazarov, *New J. Phys.* **2015**, *17*, 073018.

[37] I. Kupčić, G. Nikšić, Z. Rukelj, D. Pelc, *Phys. Rev. B* **2016**, *94*, 075434.

[38] F. J. Nelson, J.-C. Idrobo, J. D. Fite, Z. L. Mišković, S. J. Pennycook, S. T. Pantelides, J. U. Lee, A. C. Diebold, *Nano Lett.* **2014**, *14*, 3827.

[39] L. Yang, *Phys. Rev. B - Condens. Matter Mater. Phys.* **2011**, *83*, 85405.

[40] R. F. Egerton, Electron Energy-Loss Spectroscopy in the Electron Microscope, Springer US, New York, NY, USA 2011.

[41] Y. Xu, K. Zhang, C. Brüsewitz, X. Wu, H. C. Hofsäss, *AIP Adv.* **2013**, *3*, 072120.

[42] https://www.graphenea.com/.

[43] Q. M. Ramasse, *Ultramicroscopy* **2017**, *180*, 41.

[44] M. Watanabe, M. Kanno, D. Ackland, C. Kiely, D. Williams, *Microsc. Microanal.* **2007**, *13*, 1264.

[45] B. Adolph, J. Furthmüller, F. Bechstedt, *Phys. Rev. B* **2001**, *63*, 125108.

17

[46]   G. Kresse, D. Joubert, *Phys. Rev. B* **1999**, *59*, 1758.

[47]   G. Kresse, J. Furthmüller, *Phys. Rev. B* **1996**, *54*, 11169.

[48]   G. Kresse, J. Furthmüller, *Comput. Mater. Sci.* **1996**, *6*, 15.

[49]   H. Kohl, H. Rose, in Advances in Electronics and Electron Physics, Vol. 65 (Ed: P. W. Hawkes), Academic Press Inc., Orlando, FL, USA 1985, pp. 173–227.

[50] S. D. Findlay, M. P. Oxley, L. J. Allen, In *Microscopy and Microanalysis*; Cambridge University Press, 2008; Vol. 14, pp. 48–59.

[51] L. J. Allen, S. D. Findlay, M. P. Oxley, in *Scanning Transmission Electron Microscopy : Imaging and Analysis*, (Eds: S. J. Pennycook, P. D. Nellist), Springer US, New York, NY, USA **2011**, Ch. 6.

 [52] C. Koch, *PhD Thesis*, Arizona State University, May, **2002**.

Accurate control of the electronic and optical properties of graphene is key for optimal utilization in next generation devices. Modification of graphene's extreme-UV optical response induced by single atom nitrogen and boron dopants is imaged on the atomic scale using valence electron energy loss spectroscopy in the scanning transmission electron microscope.

F. S. Hage, M. D. Kapetanakis, J. -C. Idrobo, Q. M. Ramasse and D. M. Kepaptsoglou

Atomic-Scale Spectroscopic Imaging of Extreme-UV Optical Response of B and N Doped Graphene